Functional Carbon Quantum Dots as Medical Countermeasures to Human Coronavirus

Aleksandra Łoczechin,[†,‡] Karin Séron,*[,§] Alexandre Barras,[†] Emerson Giovanelli,[†] Sandrine Belouzard,[§] Yen-Ting Chen,[∥] Nils Metzler-Nolte,[‡] Rabah Boukherroub,[†] Jean Dubuisson,[§] and Sabine Szunerits*[,†]

[†]University of Lille, CNRS, Centrale Lille, ISEN, University of Valenciennes, UMR 8520 - IEMN, Lille F-59000, France

[‡]Inorganic Chemistry I, Bioinorganic Chemistry, Faculty of Chemistry and Biochemistry, Ruhr University Bochum, Universitätsstrasse 150, Bochum 44801, Germany

[§]University of Lille, CNRS, INSERM, CHU Lille, Institut Pasteur de Lille, CIIL - Center for Infection and Immunity of Lille, U1019 - UMR 8204, Lille F-59000, France

[∥]Center of Molecular Spectroscopy and Simulation of Solvent-driven Processes (ZEMOS), Ruhr-University Bochum, Bochum 44801, Germany

Ⓢ Supporting Information

ABSTRACT: Therapeutic options for the highly pathogenic human coronavirus (HCoV) infections are urgently needed. Anticoronavirus therapy is however challenging, as coronaviruses are biologically diverse and rapidly mutating. In this work, the antiviral activity of seven different carbon quantum dots (CQDs) for the treatment of human coronavirus HCoV-229E infections was investigated. The first generation of antiviral CQDs was derived from hydrothermal carbonization of ethylenediamine/citric acid as carbon precursors and postmodified with boronic acid ligands. These nanostructures showed a concentration-dependent virus inactivation with an estimated EC_{50} of 52 ± 8 μg mL^{-1}. CQDs derived from 4-aminophenylboronic acid without any further modification resulted in the second-generation of anti-HCoV nanomaterials with an EC_{50} lowered to 5.2 ± 0.7 μg mL^{-1}. The underlying mechanism of action of these CQDs was revealed to be inhibition of HCoV-229E entry that could be due to interaction of the functional groups of the CQDs with HCoV-229E entry receptors; surprisingly, an equally large inhibition activity was observed at the viral replication step.

KEYWORDS: human coronavirus (HCoV), carbon quantum dots (CQDs), antiviral therapy, boronic acid, multivalent interactions
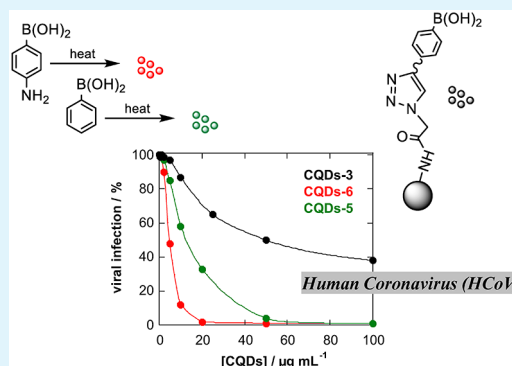
1. INTRODUCTION

The eradication of viral infections is an ongoing challenge in the medical field, not only due to the problem of spreading but also to the virus' ability to escape therapy by genetic mutations. The lack of targeted antiviral therapeutics as well as the constant emergence of new viruses make the search for antiviral agents a challenging and extremely needed research task.[1] As part of a global strategy to prevent epidemics, some severe emerging pathogens with great epidemic potential have been identified by the World Health Organization (WHO),[2] including, next to Ebola virus disease, the highly pathogenic human coronavirus (HCoV) infections. While circulating HCoVs (HCoV-229E, HCoV-OC43, HCoV-NL63, and HKU1) cause relatively mild common cold-like respiratory tract infections, severe acute respiratory syndrome coronavirus (SARS-CoV) and Middle-East respiratory syndrome coronavirus (MERS-CoV) lead to pneumonia requiring hospitalization and intensive care.[3] A total of 2266 laboratory-confirmed cases of MERS-CoV, including 804 associated deaths, have been declared to the WHO until now, with a

high case-fatality rate (35%).[4] As the virus is circulating in animals and humans, it may undergo further adaptation and cause a pandemic. Therefore, therapeutic options are urgently needed.

The current treatments for MERS-CoV are extrapolated from SARS-CoV and H1N1 influenza outbreaks.[5−7] These include different combinations of small molecules with broad antiviral activity (e.g., ribavirin, corticosteroids, and interferons (IFN)), and monoclonal and polyclonal antibody therapies.[7,8] The membrane-anchored glycoprotein S has lately been found to be essential for the interaction between the MERS-CoV and the host cell,[8,9] and the development of MERS-CoV entry/fusion inhibitors targeting the S1 subunit is nowadays considered as a viable antiviral strategy.

Recently, nanoscale materials have emerged as promising and efficient platforms to modulate the viral infection cycle.[10] Given
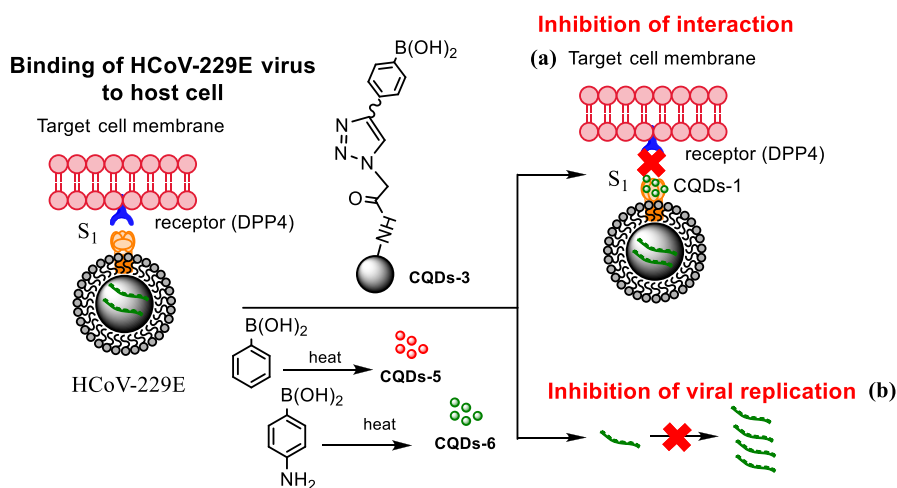
Figure 1. Influence of CQDs, prepared by hydrothermal carbonization, on binding of HCoV-229E virus to cells: (a) inhibition of protein S receptor interaction, and (b) inhibition of viral RNA genome replication.

that attachment of viruses into host cells is favored by multivalent interactions, the multivalent character of nanostructures with their high surface to volume ratio, allowing the attachment of several ligands, makes them well adapted to interfere with viral attachment and blocking viral entry into cells.

In this work, we investigate the potential of functional carbon quantum dots (CQDs) as inhibitors of host cells infection by HCoV-229E coronavirus (Figure 1). CQDs with an average diameter below 10 nm and excellent water dispersion are highly attractive for nanomedical applications due to a lack of visible signs of toxicity in animals.[11] They can be synthesized quickly via several different inexpensive and simple methods, and their excellent optical properties offer in vivo tracking possibilities. It was recently demonstrated that CQDs are suitable scaffolds to interfere with the entry of viruses into cells.[12−14] Boronic acid-modified CQDs were able to inhibit, for example, HIV-1 entry by suppressing syncytium formation.[13] Some of us have shown lately the potential of CQDs-functionalized with boronic acid and amine moieties to interfere with the entry of herpes simplex virus type 1.[12] Han and co-workers reported the potential of CQDs as viral inhibitors by activation of type I interferon responses.[14]

This unique study reveals that boronic acid functions can be responsible for the anti-HCoV activity. CQDs derived from citric acid/ethylenediamine and further conjugated by "click" chemistry with boronic acid functions display an effective 50% inhibition concentration $EC_{50} = 52 \pm 8\ \mu g\ mL^{-1}$. Likewise, CQDs derived from 4-aminophenylboronic acid and phenylboronic acid without any further modification exhibit antiviral behavior with a decreased effective EC_{50} down to $5.2 \pm 0.7\ \mu g\ mL^{-1}$. The underlying mechanism of action of these CQDs was revealed to be the CQDs interaction with the HCoV-229E S protein. Surprisingly, an equally large inhibition activity was observed at the viral replication step.

2. RESULTS AND DISCUSSION

2.1. First-Generation of CQDs Inhibitors of Host Cell Infections by HCoV-229E Coronavirus: Boronic Acid-Modified CQDs. *2.1.1. Formation and Characterization. Carbon Quantum Dots Formed from Ethylenediamine/Citric Acid.* Boronic acid derivatives have been proposed as low-toxicity agents for inhibiting the entry of various viruses.[15,16] To test if such concepts can be extrapolated to human coronavirus HCoV-229E infections, boronic acid functional groups were chemically integrated onto CQDs-1 formed through hydrothermal carbonization of ethylenediamine/citric acid (Figure 2A). The approach consists of sealing the organic precursors in a Teflon-lined autoclave chamber and performing the formation of CQDs at elevated temperature under reduced pressure for 5 h. The pH value of the resulting CQDs suspensions was found to be 7.2 ± 0.2 ($n = 5$). To remove larger precipitates, the as-obtained CQDs suspension was first centrifuged and then dialyzed against water for 24 h with a final yield of CQDs of 40%. CQDs-1 exhibit a spherical shape with an average diameter of 4.5 ± 0.2 nm (Figure 2B). XPS analysis (Table 1) indicates the presence of C, O, and N. The C_{1s} high-resolution XPS spectrum of CQDs-1 depicts three different carbon features: the graphitic C=C at 283.4 eV, 284.9 eV (C−H), and 286.4 eV (C−O, C−N) (Figure 2C). Analysis of the N_{1s} high-resolution XPS shows the presence surface NH_2 groups (399.9 eV) (Figure 2D). The Raman spectrum of the CQD-1 (Figure 2E) displays the characteristic G band at 1570 cm^{-1} related to in-plane vibration of sp^2 carbon, and the D band at 1350 cm^{-1} attributed to disorder and defects. The ratio of the intensity of these bands (I_D/I_G), used to express the extent of sp^2/sp^3 hybridization of carbon atoms,[17] is found to be 0.93 ± 0.15 for all particles.[18] XRD patterns indicate their crystalline nature (see Figure S1A) with a broad diffraction peak centered at 25.5° corresponding to an interlayer spacing of 0.35 nm. This is larger than the spacing between (100) planes in bulk graphite (0.23 nm) due to the incorporation of functional groups along the edges of the CQDs.[19] The UV−vis of CQDs-1 (see Figure S1B) reveals an absorption maximum at ~242 nm attributed to $\pi-\pi^*$ transition of C=C and a band at 344 nm due to $n-\pi^*$ transition of C=O and C=N bonds.[20,21] The fluorescence quantum yield (QY) is 0.33 as compared to that of quinine sulfate used as reference (QY, 0.54 in 0.12 M H_2SO_4) (see Figure S1C). A wavelength-dependent fluorescence emission is observed (see Figure S1D) where upon increasing the excitation wavelength, the emission gradually shifts to the red region with an increase in fluorescence intensity. The phenomenon of excitation-dependent emission is typical for such nanostructures.[5−7] The zeta potential and hydrodynamic size of the CQDs-1 are summarized in Table 1.

Functionalization of CQDs-1. The formation of CQDs-3 is based on a two-step chemical process. In a first step,
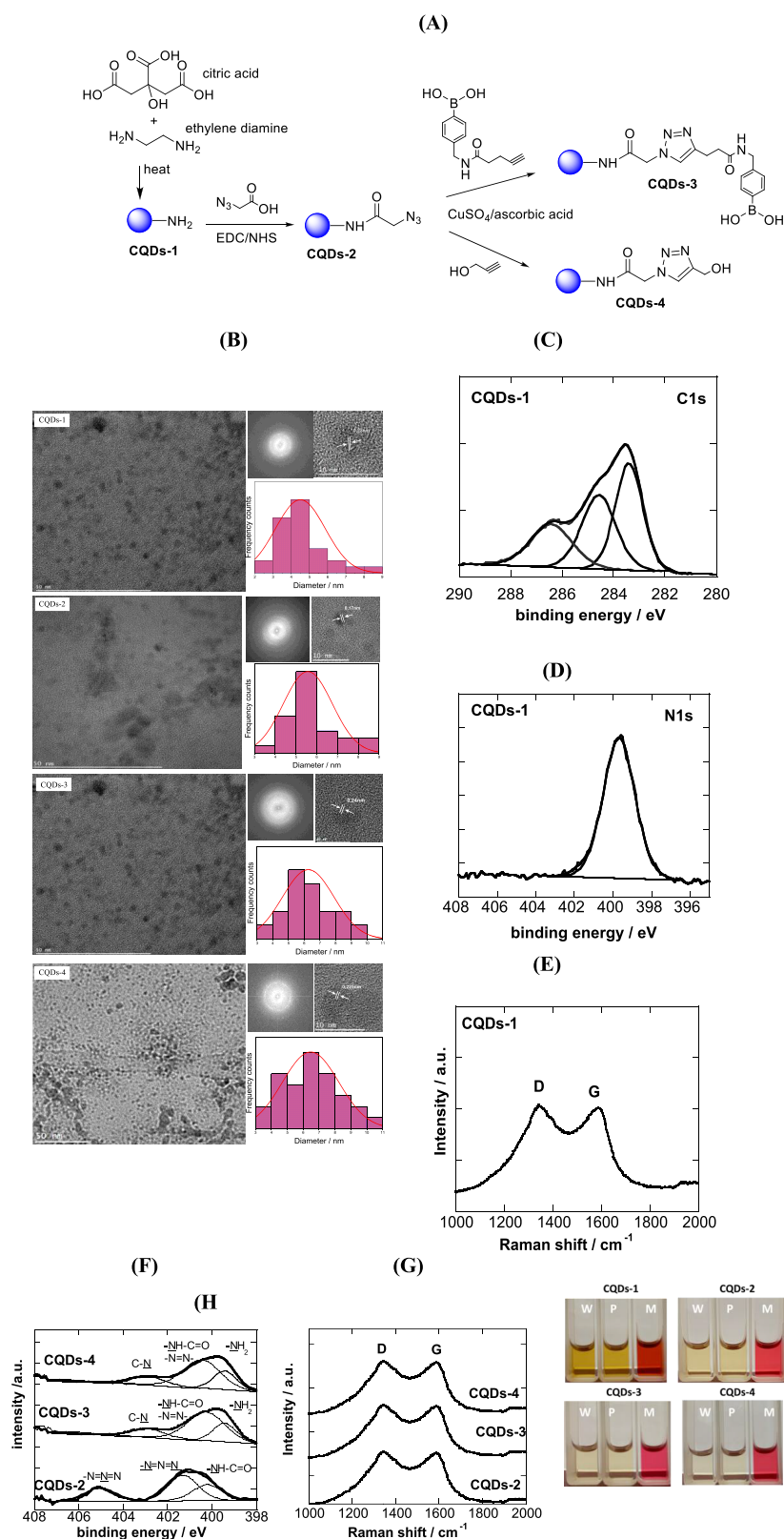
(A)

(B)   **(C)**

(D)

(E)

(F)   **(G)**

(H

Figure 2. (A) Schematic representation of the synthesis of CQDs-1−4; (B) TEM, magnified TEM, HR-TEM images, and size distribution histograms of CQDs-1−4; (C) C_{1s} high-resolution XPS spectrum of CQDs-1; (D) N_{1s} high-resolution XPS spectrum of CQDs-1; (E) Raman spectrum of CQDs-1; (F) N_{1s} high-resolution XPS spectra of CQDs-2−4; (G) Raman spectrum of CQDs-2−4; and (H) photographs of CQDs-1−4 suspensions (1 mg mL^{-1}) after 1 month in water (W), PBS (0.01 M, P), and Dulbecco's Modified Eagle's medium (M).

azido-functionalized CQDs-2 are prepared by coupling 2-azido acetic acid moieties to CQDs-1. The N_{1s} signal of CQDs-2 shows signals at 405.2 ($-N=\underline{N}^+=N^-$) and 401.6 eV

($\underline{N}=N^+=\underline{N}^-$) in a 1:2 ratio, as theoretically expected (Figure 2F). The azide functions in CQDs-2 quantitatively react with alkyne functions as indicated by the absence of the

Table 1. Physico-chemical Characteristics of the CQDs

CQDs	ζ (mV)[a]	size (nm)	hydrodynamic size (nm)[b]	PDI	C_{1s}[c] (at. %)	O_{1s} (at. %)	N_{1s} (at. %)	B_{1s} (at. %)
CQDs-1	-9.9 ± 3.4	4.5 ± 0.2	11 ± 0.1	0.22 ± 0.11	72.6	12.5	14.9	
CQDs-2	-7.9 ± 2.7	5.5 ± 0.3	12 ± 0.1	0.23 ± 0.11	68.8	13.9	17.3	
CQDs-3	-15.9 ± 4.3	6.3 ± 0.4	12 ± 0.25	0.15 ± 0.10	67.9	7.3	20.3	4.5
CQDs-4	-15.9 ± 1.3	6.5 ± 0.4	11 ± 0.19	0.13 ± 0.10	68.5	13.6	17.9	

[a]ζ, zeta potential; PDI, polydispersity index. [b]The hydrodynamic size was recorded at 37 °C. [c]XPS was used to determine the atomic percentage of the elements, respectively.

azide band at 405.2 eV in the relevant spectra of CQDs-3 and CQDs-4 (Figure 2F). The band at 399.2 eV ($-NH_2$) is most likely resulting from partial hydrolysis of surface linked 2-azido acetic ester function. CQDs-4 were synthesized as a control to check whether the triazole function acts as a passive linker or not.[22,23] The morphologies of CQDs-3 and CQDs-4 are comparable to that of CQDs-1 with an average diameter of 6.25 ± 0.17 nm (Figure 2B) and diffraction peak centered at 25.3° for CQDs-3 (see Figure S1A) and an average diameter of 6.50 ± 0.40 nm (Figure 2B), and diffraction peak centered at 25.4° for CQDs-4. The Raman spectra of the CQDs-2−4 (Figure 2G) are similar to that of CQDs-1 displaying the characteristic G and D bands with $I_D/I_G = 0.93 \pm 0.15$ for all particles.[18] The colloidal stability of CQDs-1−4 in water, phosphate buffer (PBS, 10 mM), and Dulbecco's Modified Eagle's medium (M) was, in addition, examined. All of the particles had good long-term colloidal stability as seen from the photographs in Figure 2H.

2.1.2. Cytotoxicity Assay. The cell toxicity of CQDs-1, CQDs-3, and CQDs-4 was established on Huh-7 cell lines after 8 h (time points corresponding to HCoV-229E infections) and 24 h incubation. The CQDs toxicity was evaluated using cell viability assessment by the resazurin assay, based on the conversion of nonfluorescent dye to a fluorescent molecule by mitochondrial and cytoplasmatic enzymes. All CQDs are nontoxic to Huh-7 cells even at the highest concentration (100 μg mL^{-1}) investigated when incubated for 8 and 24 h (Figure 3A). Neither the presence of boronic acid nor triazole units had a negative effect on cell toxicity.

The uptake mechanism proved to be the same for all of the nanostructures. Taking the example of CQDs-3 (which later proves to have antiviral activity), Huh-7 cells were fixed after 1 h incubation at 4 and 37 °C, and then nuclei were stained with Hoechst 33342, a fluorescent dye for labeling DNA in fluorescence microcopy (Figure 3B). The green fluorescence, which is attributed to the CQDs-3, is homogeneously distributed in the cytoplasm after 1 h when incubated at 37 °C, which confirms the internalization of CQDs-3 inside the cells. The reduction of green fluorescence, observed in the cytoplasm after 1 h incubation at 4 °C, suggests that the active internalization mechanism may be partially blocked, and a small portion of CQDs was internalized by passive penetration.

The endocytosis of CQDs-3 was, in addition, quantitatively evaluated using flow cytometry by treating Huh-7 cells with 100 μg mL^{-1} of CQDs-3 for 1 h at 4 °C and for 1, 3, and 6 h at 37 °C (Figure S2). The excitation fluorescence of CQDs-3 at 488 nm allowed analysis of CQDs intracellularly. A progressive shift in the cell population toward higher fluorescence values was observed with a subsequent increase of time incubation due to the time-dependent cellular uptake likely through endocytosis. Lower fluorescence intensity was observed upon incubation at 4 °C for 1 h, where the active uptake process is blocked. The low percentage of green cells (0.8%) observed after 1 h at 4 °C

suggests that only a very low quantity of CQDs-3 penetrates via passive uptake.

2.1.3. Antiviral Assay of First-Generation of Antiviral CQDs. The antiviral activity of CQDs-1, CQDs-3, and CQDs-4 was evaluated on Huh-7 cell monolayers, infected with HCoV-229E-Luc (Figure 4A). Addition of CQDs-1 after 1 h infection and further incubation for 6 h at 37 °C shows no inhibition of infection. This contrasts to CQDs-3 where a concentration-dependent virus inactivation is observed with an estimated EC_{50} = 52 ± 8 μg mL^{-1} (Figure 4B). Addition of mannose to CQDs-3 results in a complete loss of antiviral activity of the latter at low particle concentrations, with some antiviral activity above 50 μg mL^{-1} CQDs. These data reveal two important findings. First, it highlights that boronic acid functions, where the mode of action is the selective and reversible formation of tetravalent complexes with *cis*-diols and thus glycan units,[24] are interacting with HCoV-229E. CQDs-3 are in this context speculated to be pseudolectins, targeting the S protein of HCoV-229E via a lectin−carbohydrate binding mechanism, similar to that of the oligomannose-specific lectin Griffithsin.[25] Thus, the presence of mannose is blocking the antiviral activity in favor of this mechanistic behavior. The presence of some antiviral activity of the mannose saturated CQDs-3 might be due to the presence of the triazole function on the particles' surface. Indeed, the control particles CQDs-4, bearing no boronic acid function but a triazole ring, display some antiviral activity, even though largely decreased when compared to CQDs-3.

2.2. Second-Generation of CQDs Inhibitors of Host Cell Infections by HCoV-229E Coronavirus. *2.2.1. Formation and Characterization of CQDs-5−7.* With the aim to validate if boronic acid functions can be formed directly on CQDs, hydrothermal carbonization of phenylboronic acid and 4-aminophenylboronic acid was performed resulting in CQDs-5 and CQDs-6, respectively (Figure 5A). As control, hydrothermal carbonization of aniline and polyethylene glycol (PEG$_{600}$), both lacking boronic acid functions, was conducted. Unfortunately, several attempts to prepare CQDs from aniline as a starting material failed (see the Supporting Information for experimental details).

The TEM images of CQDs-5−7 are seen in Figure 5B. CQDs-5 have an average diameter of 9.2 ± 0.3 nm, somehow larger than CQDs-6 with an average size of 7.6 ± 0.2 nm (Table 2). The particles formed from PEG (CQDs-7) display a spherical shape with an average diameter of 8.0 ± 0.2 nm.

The XRD diffractograms (see Figure S3A) display broad diffraction peaks centered at 21.3° for CQDs-5, 22.6° for CQDs-6, and 22.1° for CQDs-7, corresponding to an interlayer spacing of 0.42 nm (CQDs-5), 0.40 nm (CQDs-6), and 0.39 nm (CQDs-7). The UV−vis absorption spectra of the CQDs are depicted in Figure S3B. The absorption shoulders at 250−300 nm correspond to a typical absorption of an aromatic π system, in accordance with the literature data.[26] The CQDs exhibit different fluorescence quantum yields (QY) of 0.03 (CQDs-5),
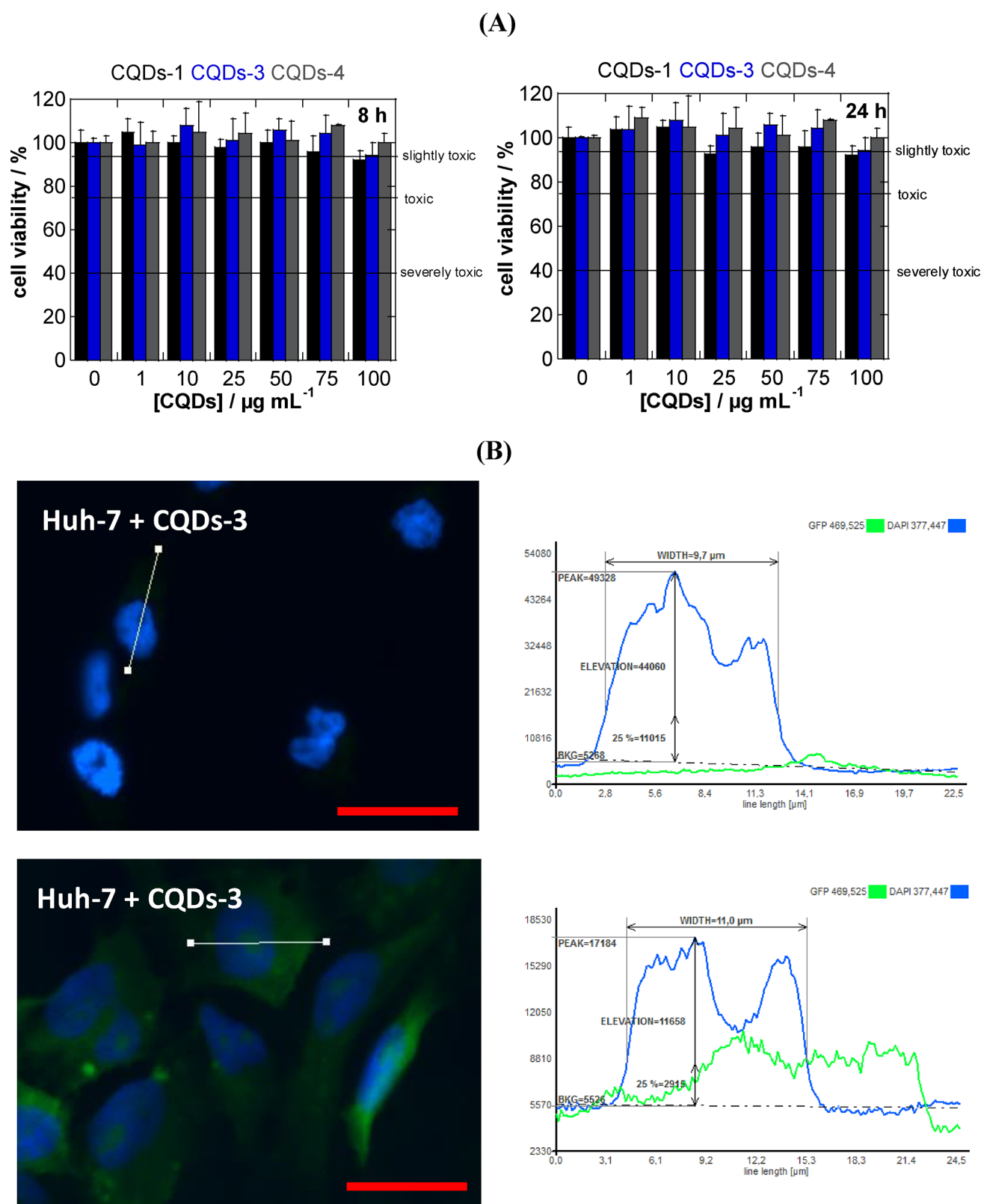
(A)

(B)

Figure 3. Characterization of postfunctionalized CQDs: (A) Viability of Huh-7 cells treated with the different CQDs. Huh-7 cells were grown in 96-well plates (15×10^3 cells/well) with 100 μL of culture medium containing increasing concentration of CQDs for 8 h (left) and 24 h (right). The results, expressed as percentage of viability, are the mean value of two independent experiments with each treatment performed in triplicate. Negative control: without CQDs. (B) Fluorescence microscopy of Huh-7 cells treated with 100 μg mL^{-1} of CQDs-3 for 1 h at 4 °C (upper) and 37 °C (lower). The blue signal corresponds to the nuclei stained with Hoechst 33342, while the green signal is attributed to CQDs-3. Scale bars = 50 μm.

0.05 (CQDs-6), and 0.09 (CQDs-7) (Figure S3C). The wavelength-dependent fluorescence emission properties of the CQDs are comparable (Figure S3D). The zeta potential and hydrodynamic size of CQDs-5−7 are summarized in Table 2. Raman spectra of
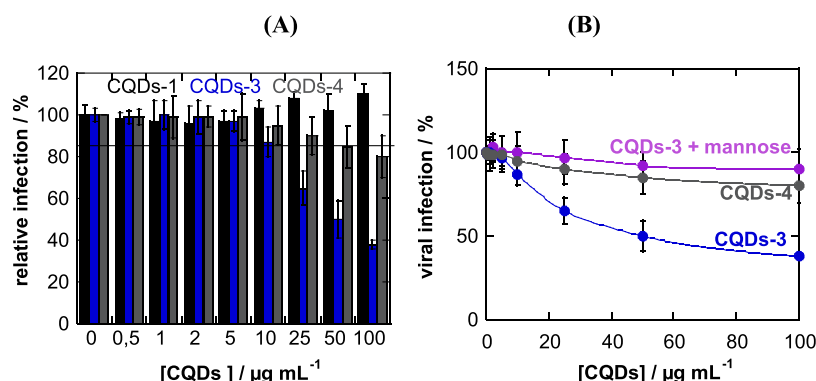
Figure 4. Viral infection inhibition in the presence of CQDs: (A) Viral inhibition using CQDs at various concentrations. Huh-7 cells (1.5×10^4 cells/well) were inoculated with HCoV-229E-Luc for 1 h (in atmosphere with 5% CO_2 at 37 °C) in the presence or absence of different CQDs in medium without FBS for 1 h. Afterward, the inoculum was removed and replaced by DMEM with FBS for 6 h. Cells were lysed, and luciferase activity was quantified. The results are expressed as percentage of infection normalized to the control without CQDs, which is expressed as 100% infection. Data are means of two independent experiments with each treatment performed in triplicate. (B) Determination of EC_{50} for CQDs-3 and CQDs-4, and effect of viral inhibition using CQDs-3 after incubation with mannose (2:1) overnight at 4 °C.

the CQDs-5−7 (Figure S3E) are comparable to that of CQDs-1 displaying the characteristic G and D band with $I_D/I_G = 0.93 \pm 0.15$ for all particles.

The chemical composition of the particles was thus further assessed using X-ray photoelectron spectroscopy and ^{11}B NMR. The XPS survey spectra of different CQDs (Table 2) indicate the presence of C_{1s}, O_{1s}, N_{1s}, and B_{1s} in agreement with the chemical composition of the particles. Deconvolution of the C_{1s} XPS spectrum of CQDs-5 reveals bands located at 284.3 eV (C=C, sp^2), 285.1 eV (C−H, C−B), and a small contribution centered at 287.0 eV (C=O) (Figure 5C). The boron content is lower than that reported by Shen and Xi,[27] but comparable to that reported by Wang et al.[28] This indicates that some of the phenylboronic acid groups were carbonized under our experimental conditions. The low B content might also indicate doping rather than the presence of boronic acid function. CQDs-6 particles depict bands at 284.3 eV (C=C, sp^2), 285.2 eV (C−H, C−B), 287.3 eV (C=O), and a band at 290.3 eV due to O−C=O functions. In the case of CQDs-7, the C_{1s} XPS spectrum comprises three different carbon features: the graphitic C=C at 283.4 eV, 284.9 eV (C−H), and 286.4 eV (C−O, C−N). Analysis of the N_{1s} high-resolution spectrum of CQDs-5 reveals the presence of surface −NH$_2$ groups (Figure 5D).

The FTIR spectra (Figure 5E) of CQDs-5−7 exhibit a distinct band at 3465 cm^{-1} attributed to the stretching vibration of −OH groups and bands at around 2874 and 2924 cm^{-1} due to CH$_2$ stretching bands. The sharp band at 1618 cm^{-1} is assigned to graphitic C=C, and the C−H deformation mode is seen at 1460 cm^{-1}. The C=O band at ∼1780−1650 cm^{-1} is also visible in all cases. In the case of CQDs-6, the band at 1090 cm^{-1} might be due to C−B stretching modes. This band is less defined in the case of CQDs-5, which might underline doping rather than presence of boronic acid functions. The FTIR spectrum of CQDs-7 displays the C−O−C bands of the PEG units at 1043 cm^{-1}.

CQDs-5−7 exhibited a negative zeta potential in water (pH 7.4) at room temperature and showed excellent long-term stability even in biological medium such as Dulbecco's Modified Eagle's medium (M) (Figure 5F).

The cytotoxicity of CQDs-5−7 (Figure 6) is comparable to that of CQDs discussed before (Figure 3), with CQDs-6 being slightly more toxic at concentrations >25 μg mL^{-1} after 24 h incubation. This might be due to the presence of NH$_2$ groups on

these particles. The uptake mechanism of these particles was comparable and is exemplified using CQDs-6 in Figure S4. Because of low intrinsic fluorescence of CQDs-6 particles, they were labeled with fluorescein-NHS.

2.2.2. Antiviral Assay of the Second-Generation of CQDs-5−7. Addition of CQDs-7 after 1 h infection and further incubation for 6 h at 37 °C showed no inhibition of infection (Figure 7A), indicating that these particles are not interfering with HCoV-229E-Luc entry or replication. CQDs-5 and CQDs-6 display a concentration-dependent virus inactivation. The dose−response curve (Figures 7B) reveals that the effective concentration to achieve 50% inhibition (EC_{50}) against HCoV-229E-Luc infection is 5.2 ± 0.7 μg mL^{-1} for CQDs-6 and 11.6 ± 1.1 μg mL^{-1} for CQDs-5. Surprisingly, addition of mannose did not result in a loss of the antiviral activity (Figure 7C), as observed previously for CQDs-3.

Performing ^{11}B NMR analysis of CQDs-5 and CQDs-6 (Figure 7D) and comparing the obtained spectra to those of the respective starting materials, 4-aminophenylboronic acid and phenyl boronic acid (Figure 7E), reveal large differences in chemical composition. 4-Aminophenylboronic acid and phenyl boronic both exhibit a strong signal at around 29 ppm, in accordance with literature data for −B(OH)$_2$ functions.[29,30] The small signal at about 20 ppm arises most likely from residual B(OR)$_3$ often used in boronic acid synthesis.[31] The ^{11}B NMR spectra of CQDs-5 and CQDs-6 display, however, peaks at 13 ppm (CQDs-5) and a band at 10 ppm with a shoulder at 12 ppm for CQDs-6. This means that boron was incorporated through doping rather than surface functionalization, during the hydrothermal reaction. Indeed, one-pot solvothermal synthesis using aminophenylboronic acid precursor was reported by Wang et al. to result in N and B codoped CQDs.[32] They indeed reported the presence of 0.7 at. % B by XPS comparable to the amount obtained here (Table 2).

2.3. Mechanism of Action. We further investigated the mechanism of action of CQDs-3 and CQDs-6 on viral infection by performing a time-of-addition assay. CQDs (at 10 μg mL^{-1}) were added at different time points during infection, as represented in Figure 8A. As expected, a strong inhibition of infection was observed when CQDs were added after 1 h inoculation. Moreover, the inhibition activity of CQDs was stronger when the nanoparticles were added during the entry step, that is, 30 minutes before and after inoculation and during inoculation.
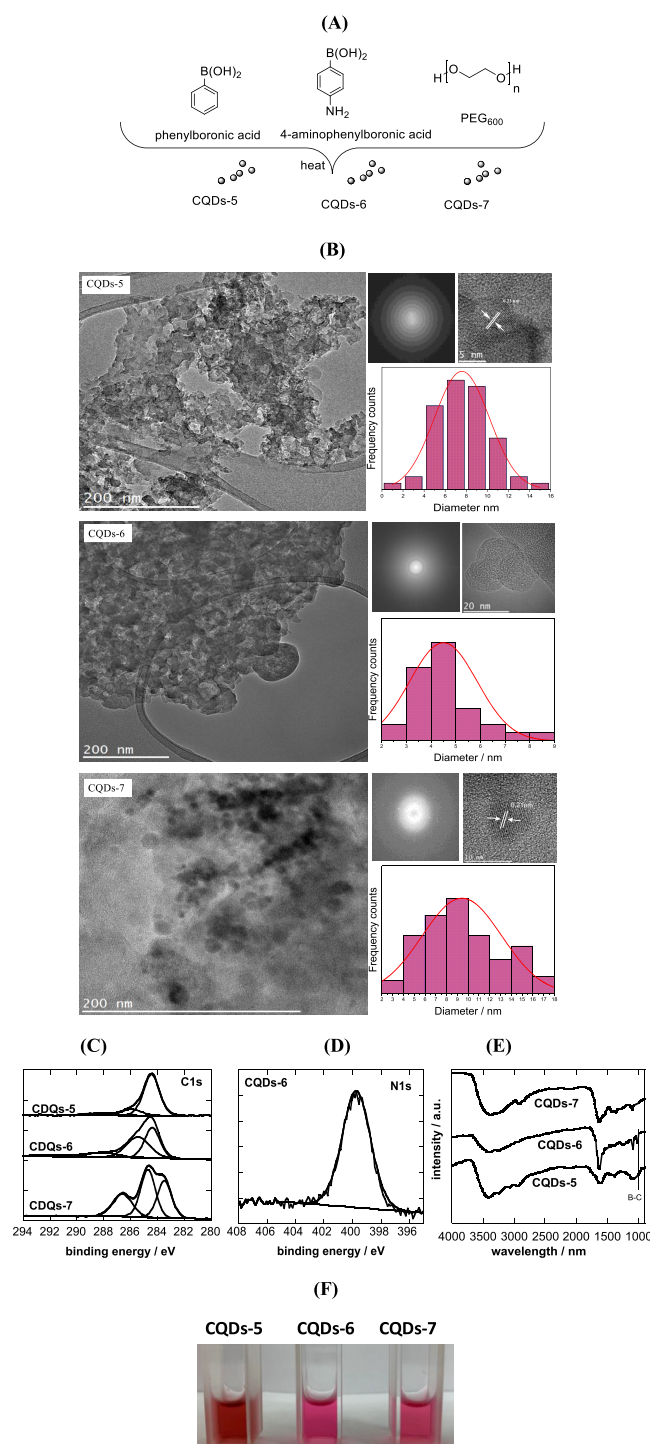
Figure 5. Chemical composition of the CQDs-5−7: (A) Schematic representation of the hydrothermal carbonization of different organic precursors for the synthesis of CQDs-5−7; (B) TEM, magnified TEM, and size distribution histograms of CQDs-5−7; (C) C_{1s} high-resolution XPS spectrum of CQDs-5−7; (D) N_{1s} high-resolution XPS spectrum of CQDs-6; (E) FTIR spectra of CQDs-5−7; and (F) photographs of CQDs-5−7 suspensions (1 mg mL^{-1}) after 1 month in Dulbecco's Modified Eagle's medium (M).

These results agree with our hypothesis of an interaction of CQDs with HCoV-229E S protein, or an interaction of CQDs with entry factors. Surprisingly, a strong inhibitory activity of CQDs was also observed when they were added after 5.5 h after the entry step, the replication step. The inhibition is

not significantly different for the entry step as compared to the replication step. This suggests that, in addition to its major effect on HCoV-229E entry, CQDs can also affect the genomic replication of this virus. This could potentially be explained by an interaction between the CQDs and a cell surface protein leading to signal transduction affecting viral replication, or by an interaction with cytosolic proteins as CQDs are internalized.

To determine if CQDs are interacting directly with viral particles, HCoV-229E-Luc was incubated with CQDs at 10 μg mL^{-1} for 30 min at 37 °C before inoculation. The inoculum was diluted 10 times, leading to a final concentration of CQDs of 1 μg mL^{-1}, and infection assay was performed. In parallel, Huh-7 cells were inoculated with HCoV-229E-Luc in the presence of CQDs at 1 or 10 μg mL^{-1}. The inoculum titers were kept constant in the different conditions. The results showed that the preincubation of the virus with CQDs at high concentration does not impair HCoV-229E infection, meaning that CQDs are not interacting with the particles before infection (Figure 8B). Taken together, our results are in favor of an interaction of CQDs with cellular factors that may explain their antiviral effects at different steps of infection.

3. CONCLUSION

The viral infection cycle produces important biological and structural changes in the host cell, resulting in cell damage. The possibility to interfere with viral attachment to cells as well as viral replication to reduce viral infection and spreading is an appropriate antiviral approach. We presented here the antiviral performance of seven different CQDs with their main features summarized in Table 3. Three of these CQDs (CQDs-3, -5, -6) were shown to interfere significantly with HCoV-229E-Luc infection in a concentration-dependent manner, while CQDs-4 showed a very moderate antiviral activity. The estimated EC$_{50}$ value decreased considerably from CQDs-3, boronic acid-modified quantum dots, derived from ethylenediamine/citric acid as carbon precursors (EC$_{50}$ = 52 ± 8 μg mL^{-1}) to 5.2 ± 0.7 μg mL^{-1} in the case of CQDs-6. While the presence of boronic acid functions proved to be vital for covering CQDs-3 with antiviral activity, CQDs-5 and CQDS-6 did not carry a substantial amount of boronic acid functions, as revealed by ^{11}B NMR and validated by mannose addition experiments. These findings reveal the complex nature of identifying viral inhibitors for human coronaviruses such as HCoV-229E-Luc. Mechanistic studies suggest that the particles are acting at the early state of virus infection through the inhibition of entry that could be due to inhibition of protein S-receptor interaction with the host cell membrane. All different particles interfere in addition with the viral replication step, something less common. These results are extremely encouraging to replace currently used antiviral agents such a ribavirin and IFN known to have major side effects such as confusion, short-term memory loss, deficits in executive functions, as well as extrapyramidal effects. Further experimental confirmations are required if this approach can be extrapolated to other coronaviruses, notably to the clinically relevant MERS-CoV, to validate the potential of these nanostructures as alternative anti-MERS therapeutics and approaches to confront this severe and life-threatening disease. Also, how such particles work in vivo has to be shown in the future.

4. EXPERIMENTAL SECTION

4.1. Materials. Citric acid, ethylenediamine, 4-aminophenylboronic acid, phenylboronic acid, poly(ethylene glycol) (PEG600, molecular

Table 2. Physico-chemical Characteristics of the CQDs-5−7

CQDs	ζ (mV)[a]	size (nm)	hydrodynamic size (nm)[b]	PDI	C_{1s}[c] (at. %)	O_{1s} (at. %)	N_{1s} (at. %)	B_{1s} (at. %)
CQDs-5	-20.0 ± 5.5	7.6 ± 0.2	13 ± 1.8	0.14 ± 0.09	77.4	21.7		0.9
CQDs-6	-41.2 ± 1.0	9.2 ± 0.3	12 ± 0.2	0.11 ± 0.06	69.4	21.5	7.4	1.7
CQDs-7	-39.2 ± 1.5	8.0 ± 0.2	13 ± 3.1	0.28 ± 0.34	60.8	39.2		

[a]ζ, zeta potential; PDI, polydispersity index. [b]The hydrodynamic size was recorded at 37 °C. [c]XPS was used to determine the atomic percentage of the elements, respectively.
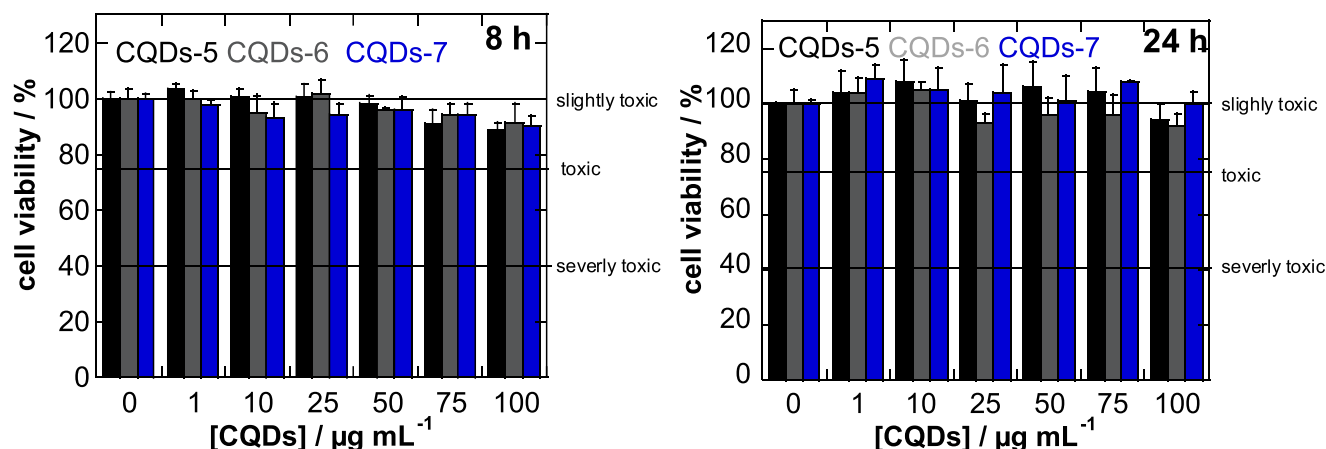

Figure 6. Cell viability of CQDs-5−7: Viability of Huh-7 cells grown in 96-well plates (15×10^3 cells/well) with 100 μL of culture medium containing increasing concentration of CQDs-5−7 for 8 and 24 h. The results, expressed as percentage of viability, are the mean value of two independent experiments with each treatment performed in triplicate. Negative control: without CQDs.
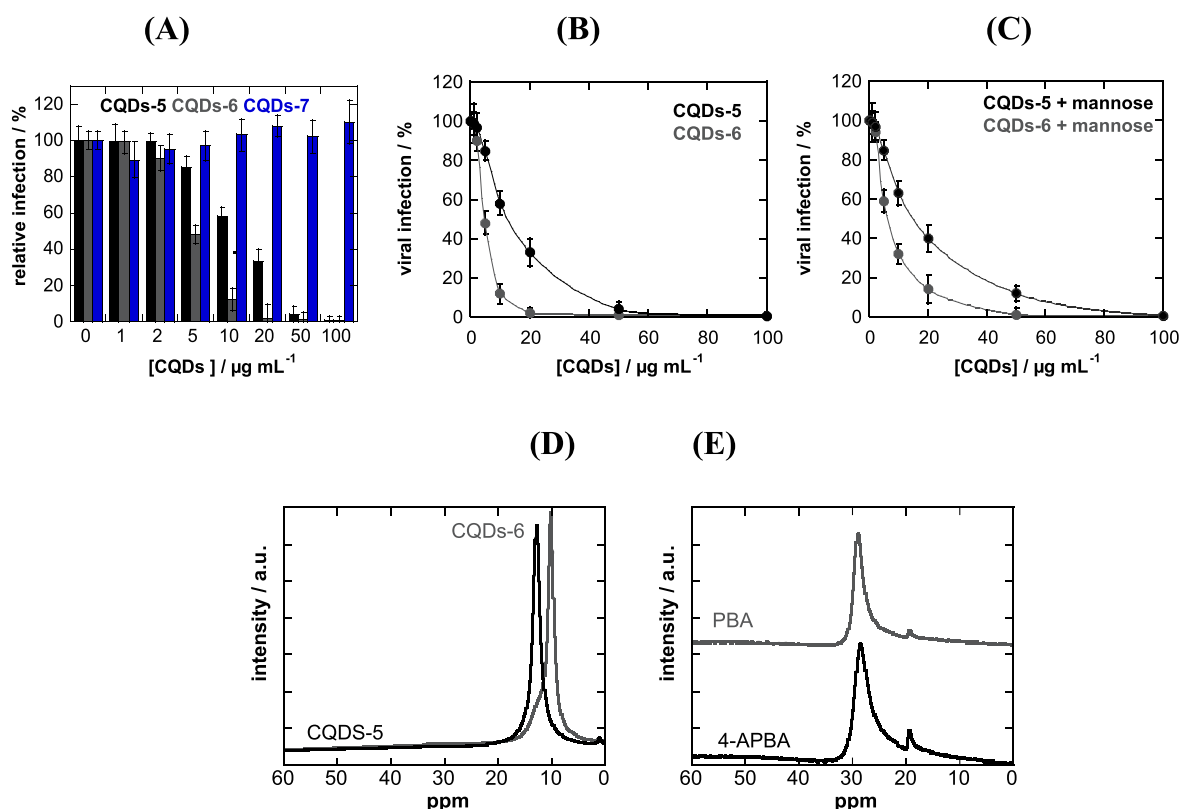

Figure 7. Viral infection inhibition in the presence of CQDs-5−7: (A) Viral inhibition using CQDs-5−7 at various concentrations. Huh-7 cells (1.5×10^4 cells/well) were inoculated with HCoV-229E-Luc for 1 h (in atmosphere with 5% CO_2 at 37 °C) in the presence or absence of different CQDs in medium without FBS for 1 h. Afterward, the inoculum was removed and replaced by DMEM with FBS for 6 h. Cells were lysed, and luciferase activity was quantified. The results were expressed as percentage of infection normalized to the control without CQDs, which is expressed as 100% infection. Data are means of two independent experiments with each treatment performed in triplicate. (B) Determination of EC_{50} for CQDs-5 and CQDs-6. (C) Viral inhibition using CQDs-5 and CQDS-6 after incubation with mannose (2:1) overnight at 4 °C. (D) ^{11}B NMR spectra of CQDs-5 and CQDs-6 prepared by hydrothermal method from phenyl boronic acid (PBA) and 4-aminophenylboronic acid (4-APBA) precursors, respectively. (E) ^{11}B NMR spectra of 4-aminophenylboronic acid (4-APBA) and phenyl boronic acid (PBA) starting materials.
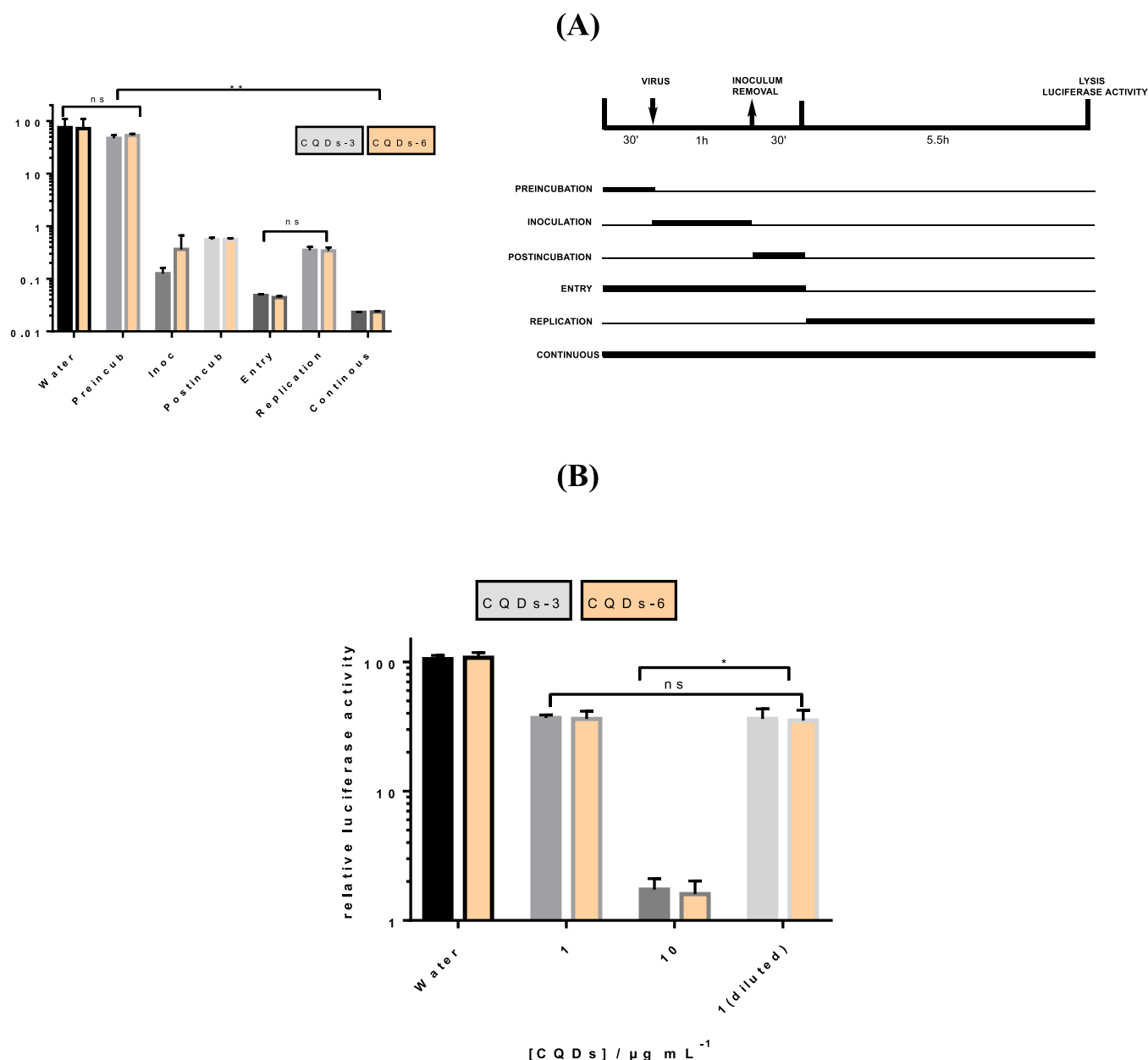
Figure 8. Time-of-addition assay of CQDs-3 and -6 during HCoV-229E infection. (A) CQDs at 10 μg mL^{-1} were added at different time points during infection of Huh-7 cells with HCoV-229E-Luc as shown below the graph. Cells were lysed, and luciferase activity was quantified. Results are representative of three experiments performed in triplicate. Error bars represent SD of three independent values. (B) Virus HCoV-229E-Luc was preincubated with CQDs at 10 μg mL^{-1} for 30 min at 37 °C. The mixture was diluted 10 times in culture medium leading to a final concentration of CQDs of 1 μg mL^{-1}, and inoculated on Huh-7 cells for 1 h. In parallel, Huh-7 cells were inoculated with HCoV-229E-Luc in the presence of CQDs at 1 and 10 μg mL^{-1} for 1 h. Cells were lysed 7 h postinfection and luciferase activity quantified. Results are means of three experiments performed in triplicate. Error bars represent means of three independent values. Statistic evaluation (confidence interval of 95%), ns ($p > 0.99$); * ($p < 0.1$); ** ($p < 0.01$).

weight 570−630), *N*-(3-(dimethylamino)propyl)-*N'*-ethylcarbodiimide hydrochloride (EDC), *N*-hydroxysuccinimide (NHS), propargyl alcohol, 4-pentynoic acid, copper sulfate pentahydrate, L-ascorbic acid, and sodium hydroxide were purchased from Sigma-Aldrich. The dialysis membranes were supplied by Spectrum Laboratories.

4.2. Synthesis of Functional Carbon Quantum Dots (CQDs). *CQDs-1.* Particles were synthesized following a method similar to that reported by Zhu et al.[33] (see Supporting Information SI1 for more details). The details about the characterization instruments can be found in Supporting Information SI2.

CQDs-2. Azide-terminated CQDs-2 were obtained from CQDs-1 by the use of carbodiimide chemistry. To a solution of 2-azidoacetic acid (1 mg mL^{-1}, 0.1X PBS) was added an equimolar amount of EDC·HCl and NHS, and the solution was stirred for 20 min to activate the

carboxyl group. To this solution was added CQDs-1 (1 mg mL^{-1}, 0.1X PBS) in a 1:2 volume ratio (v/v). The reaction was carried out for 5 h at room temperature, and the resulting solution was then dialyzed against Milli-Q water using cellulose ester dialysis membrane for 24 h (Biotech CE no. 131093, molecular weight cutoff 500−1000 Da) to remove unreacted material.

CQDs-3. CQDs-2 were further reacted with "clickable" phenyl boronic acid derivative 4-[(1-oxo-4-pentyn-1-yl)amino]phenylboronic acid, synthesized as reported previously.[34] For this, CQDs-2 (1 mg mL^{-1}, 5 mL) were mixed with 4-[(1-oxo-4-pentyn-1-yl) amino] phenyl-boronic acid (2 mM), copper sulfate pentahydrate (200 μM), and ascorbic acid (300 μM). The reaction mixture was stirred for 24 h at room temperature. EDTA was added to the mixture prior to dialysis (SpectraPor 1, pore size: 1000 Da) against Milli-Q water for 48 h.

Table 3. Summary of the Main Features of CQDs-1−7

CQDs	size (nm)	charge	functions	antiviral	$EC_{50}/\mu g\ mL^{-1 a}$
CQDs-1	4.5 ± 0.2	−9.9	NH_2, COO^-	−	
CQDs-2	5.5 ± 0.3	−7.9	N_3	−	
CQDs-3	6.3 ± 0.4	−15.9	triazole, $R-B(OH)_2$	++	52 ± 8
CQDs-4	6.5 ± 0.4	−15.9	triazole, OH	+	n.d.
CQDs-5	7.6 ± 0.2	−20.0	$R-B(OH)_2$	+++	11.6 ± 1.1
CQDs-6	9.2 ± 0.3	−41.2	$R-B(OH)_2$, NH_2	++++	5.2 ± 0.7
CQDs-7	8.0 ± 0.3	−39.2	PEG	−	

[a] nd, not determinable.

CQDs-4. CQDs-2 were further reacted with commercially available propargyl alcohol. For this, CQDs-2 (1 mg mL^{-1}, 5 mL) were mixed with propargyl alcohol (2 mM), copper sulfate pentahydrate (200 μM), and ascorbic acid (300 μM). The reaction mixture was stirred for 24 h at room temperature. EDTA was added to the mixture prior to dialysis (SpectraPor 1, pore size: 1000 Da) against Milli-Q water for 48 h.

CQDs-5 and CQDS-6. Particles were prepared according to the protocol recently described by us.[12]

CQDs-7. Particles were prepared in a manner similar to that for CQDs-2 by dissolving PEG600 (200 mg) in water (20 mL) and adjusting the pH to 9.0 by adding NaOH (0.5 M). The solution was degassed with nitrogen gas during 1 h to remove dissolved oxygen and heated in a Teflon-lined autoclave chamber (125 mL − acid digestion vessel no. 4748, Parr, France) for 72 h at 120 °C. After being cooled to room temperature, the solution was dialyzed against water for 24 h with water being changed every 6 h (SpectraPor 1, pore size: 3500 Da).

4.3. Biological Assays. *Cell and Toxicity Assay.* The Huh-7 hepatocarcinoma cell line was cultured and maintained in Dulbecco's Modified Eagle's medium (DMEM, Gibco) supplemented with 10% fetal bovine serum (FBS, Gibco) and 1% penicillin-streptomycin (Gibco) in a humidified incubator at 37 °C and 5% CO_2. Cells were seeded at a density of 15×10^3 cells/well in a 96-well plate and grown for 24 h before assay. The culture medium was replaced with a fresh medium that contains increasing concentrations of CQDs for 2 and 8 h from 1 to 100 μg mL^{-1}. The old medium was then aspirated, and cells were washed with PBS. The cell viability was evaluated using resazurin cell viability assay. Briefly, 100 mL of the resazurin solution (11 μg mL^{-1}) in DMEM/10% FBS was added to each well, and the plate was incubated for 4 h in the humidified incubator. The fluorescence emission of each well was measured at 593 nm (20 nm bandwidth) with an excitation at 554 nm (18 nm bandwidth) using a Cytation 5 Cell Imaging Multi-Mode Reader (BioTek Instruments SAS, France). Each condition was replicated three times, and the mean fluorescence value of nonexposed cells was taken as 100% cellular viability.

Fluorescent Labeling of CQDs: Uptake Mechanism. To study the uptake mechanism of the particles into cells, CQDs were dissolved in PBS buffer (pH 7.4) at the concentration of 2 mg mL^{-1}. Fluorescein-NHS was dissolved in DMF (10 mg mL^{-1}). A solution of CQDs-5 was cooled to 0 °C, and 10 μL of freshly prepared fluorescein-NHS solution was added. The reaction was stirred on ice for another 3 h. To remove the excess of the fluorescein dye, a Sephadex G-25 PD-10 desalting column was used. Cells were seeded at a density of 15×10^4 cells/well in a 24-well plate with sterile coverslips at the bottom and grown for 24 h before assay. The culture medium was replaced with a fresh medium that contained 100 μg mL^{-1} of CQDs. After 1 h incubation at 4 and 37 °C, the Huh-7 cells were washed with PBS (three times), fixed with 4% paraformaldehyde for 10 min at room temperature, and then stained with 10 μg mL^{-1} Hoechst 33342 in PBS for 10 min at room temperature in the dark. After being washed with PBS, the coverslips were mounted on glass slides and recorded using a Cytation 5 Cell Imaging Multi-Mode Reader (BioTek Instruments SAS, France) equipped with 40× objective (Plan Fluorite WD 2.7 NA 0.6). The fluorescence images were acquired with the same exposure using DAPI (377/447 nm) and GFP (469/525 nm) excitation/emission filter sets. All of the images were processed using Gen5 Image+ software.

For cellular uptake, cells were seeded at a density of 15×10^4 cells/well in a six-well plate and grown for 48 h before assay. The culture medium was replaced with a fresh medium that contained 100 μg mL^{-1} of CQDs. After 1 h incubation at 4 °C and 1, 3, and 6 h incubation at 37 °C, the Huh-7 cells were washed with PBS (three times) and collected by trypsinization. The cells suspensions were resuspended in PBS/PFA 0.5% and analyzed through a flow cytometer (BD LSR Fortessa) with FITC channel. The data were collected (10^4 cells per sample) and analyzed using BD FACSDiva 8.0.1 software.

Antiviral Assay: HCoV-229E-Luc. We used a modified HCoV-229E containing a renilla luciferase reporter gene HCoV-229E-Luc. The viral stocks were produced in Huh-7 cells. Huh-7 cells were infected with a prestock of HCoV-229E-Luc in flasks. After 5 days, the supernatants of flasks were collected. For infection assay, Huh-7 cells, 15 000/well seeded in 96-well plate, were inoculated with HCoV-229E-Luc at a multiplicity of infection (MOI) of 1 during 1 h at 37 °C in DMEM without serum, and then the inoculum was removed and cells were incubated in complete culture medium for 6 h at 37 °C. CQDs were added to cells during the 1 h of infection. Cells were lysed in 20 μL of Renilla Lysis Buffer (Promega, Madison, WI) and luciferase activity quantified using a Renilla Luciferase Assay System kit (Promega, Madison, WI) as recommended by the manufacturer and a Tristar LB 941 luminometer (Berthold Technologies, Bad Wildbad, Germany). To measure EC_{50}, dose−response experiment was performed with CQDs added at different concentrations during inoculation step and postinoculation step. For time-of-addition assays, CQDs were added at different time points at 10 μg mL^{-1}. For all experiments, water was used as a control because CQDs are diluted in water.

Statistical Analysis. The statistical test used is a Mann−Whitney nonparametric with a confidence interval of 95%. The data were analyzed using GraphPad Prism (version 5.0b) by comparison between treated and untreated groups (DMSO control). P values of 0.05 were considered to be significantly different from the control.

■ ASSOCIATED CONTENT

Ⓢ Supporting Information

The Supporting Information is available free of charge on the ACS Publications website at DOI: 10.1021/acsami.9b15032.

> Synthesis of functional cation quantum dots (CQDs-1, CQDs-5, CQDS-6) as well as the synthesis of CQDs from aniline (S1); description of methods used for the characterization of CQDs (S2); XRD diffractograms, UV-vis absorption spectra, fluorescence spectra and wavelength-dependent fluorescence emission properties of the different CQDs (Figure S1); XPS of flow cytometry analysis (Figure S2); XRD diffractograms, UV-vis spectra, fluorescence spectra, wavelength-dependent fluorescence and Raman spectra of CQDs 5-7; fluorescence images of Huh-7 cells treated with CQDs-6 (PDF)

■ AUTHOR INFORMATION

Corresponding Authors

*E-mail: sabine.szunerits@univ-lille.fr.
*E-mail: karin.seron@ibl.cnrs.fr.

ORCID Ⓘ

Alexandre Barras: 0000-0003-2821-7079
Emerson Giovanelli: 0000-0001-9097-9301
Nils Metzler-Nolte: 0000-0001-8111-9959
Rabah Boukherroub: 0000-0002-9795-9888
Sabine Szunerits: 0000-0002-1567-4943

Notes

The authors declare no competing financial interest.

Research Article

■ ACKNOWLEDGMENTS

■ REFERENCES

(1) Nii-Trebi, N. I. Emerging and Neglected Infectious Diseases: Insights, Advances, and Challenges. *BioMed Res. Int.* **2017**, *2017*, 1−15.

(2) http://www.who.int/csr/research-and-development/meeting-report-prioritization.pdf (accessed 16 September 2019).

(3) Al Hajjar, S.; Ziad A. Memish, Z. A.; McIntosh, K. Middle East Respiratory Syndrome Coronavirus (MERS-CoV): A Perpetual Challenge. *Ann. Saudi Med.* **2013**, *33*, 427−436.

(4) http://www.emro.who.int/pandemic-epidemic-diseases/mers-cov/mers-situation-update-november-2017.html (accessed 16 September 2019).

(5) Mo, Y.; Fisher, D. A Review of Treatment Modalities Of Middle Repsiratorey Syndroms. *J. Antimicrob. Chemother.* **2016**, *71*, 3340−3350.

(6) Uyeki, T. M.; Erlandson, K. J.; Korch, G.; O'Hara, M.; Wathen, M.; Hu-Primmer, J.; Hojvat, S.; Stemmy, E. J.; Donabedian, A. Development of Medical Countermeasures to Middle East Respiratory Syndrome Coronavirus. *Emerging Infect. Dis.* **2016**, *22*, 1−6.

(7) Zumla, A.; Chan, J. F. W.; Azhar, E. I.; Hui, D. S. C.; Yuen, K.-Y. Coronavirus-Drug Discovery and Therapeutic Options. *Nat. Rev. Drug Discovery* **2016**, *15*, 327−347.

(8) Du, L.; Yang, Y.; Zhou, Y.; Lu, L.; Li, F.; Jiang, S. MERS-Cov Spike Protein: A Key Target for Antivirals. *Expert Opin. Ther. Targets* **2017**, *21*, 131−143.

(9) Lu, L.; Liu, Q.; Zhu, Y.; Chan, K.-H.; Qin, L.; Li, Y.; Wang, Q.; Chan, J. F. W.; Du, L.; Yu, F.; Ma, C.; Ye, S.; Yuen, K.-Y.; Zhang, R.; Jiang, S. Structures-Based Discovery Of Middle East Repiratory Syndrome Coronavirus Fusion Inhibitor. *Nat. Commun.* **2014**, *5* (3067), 1−15.

(10) Szunerits, S.; Barras, A.; Khanal, M.; Pagneux, Q.; Boukherroub, R. Nanostructures for the Inhibition of Viral Infections. *Molecules* **2015**, *20*, 14051−14081.

(11) Lim, S. Y.; Shen, W.; Gao, Z. Carbon Quantum Dots And Their Applications. *Chem. Soc. Rev.* **2015**, *44*, 362−381.

(12) Barras, A.; Pagneux, Q.; Sane, F.; Wang, Q.; Boukherroub, R.; Hober, D.; Szunerits, S. High Efficiency of Functional Carbon Nanodots as Entry Inhibitors of Herpes Simplex Virus Type 1. *ACS Appl. Mater. Interfaces* **2016**, *8*, 9004−9013.

(13) Fahmi, M. Z.; Sukmayani, W.; Qamariyah Khairunisa, S.; Witaningrum, A. M.; Indriati, D. W.; Matondang, M. Q. Y.; Chang, J.-Y.; Kotaki, T.; Kameokaf, M. Design of boronic acid-attributed carbon dots on inhibits HIV-1 entry. *RSC Adv.* **2016**, *6*, 92996−93002.

(14) Du, T.; Liang, J.; Dong, N.; Liu, L.; Fang, L.; Xiao, S.; Ha, H. Carbon Dots As Inhibitors Of Virus By Activation Of Type I Interferon Response. *Carbon* **2016**, *110*, 278−285.

(15) Trippier, P. C.; Balzarini, J.; C. McGuigan, A. Phenylboronic-Acid-Based Carbohydrate Binders As Antiviral Therapeutics: Bisphenylboronic Acids. *Chem. Chemother.* **2011**, *21*, 129−142.

(16) Khanal, M.; Barras, A.; Vausselin, T.; Fénéant, L.; Boukherroub, R.; Siriwardena, A.; Dubuisson, J.; Szunerits, S. Boronic Acid-Modified Lipid Nanocapsules: A Novel Platform For The Highly Efficient Inhibition Of Hepatitis C Viral Entry. *Nanoscale* **2015**, *7*, 1392−1402.

(17) Gupta, V.; Chaudhary, N.; Srivastava, R.; Sharma, G. D.; R. Bhardwaj, R.; S. Chand, S. Luminscent Graphene Quantum Dots for Organic Photovoltaic Devices. *J. Am. Chem. Soc.* **2011**, *133*, 9960−9963.

(18) Yaoping, H.; Jing, Y.; Jiangwei, T.; Jun-Sheng, Y. How Do Nitrogen-Doped Carbon Dots Generate From Molecular Precursors? An Investigation Of The Formation Mechanism And A Solution-Based Large-Scale Synthesis. *J. Mater. Chem. B* **2015**, *3*, 5608−5614.

(19) Hu, C.; Liu, Y.; Yang, Y.; Cui, J.; Huang, Z.; Wang, Y.; Yang, L.; Wang, H.; Xiao, Y.; Rong, J. One-Step Preparation Of Nitrogen-Doped Graphene Quantum Dots From Oxidized Debris Of Graphene Oxide. *J. Mater. Chem. B* **2013**, *1*, 39−42.

(20) Wang, S.; Cole, I. S.; Zhao, D.; Li, Q. The Dual Roles Of Functional Groups In The Photoluminescence Of Graphene Quantum Dots. *Nanoscale* **2016**, *8* (14), 7449−7458.

(21) Kim, T. H.; White, A. R.; Sirdaarta, J. P.; Ji, W.; Cock, I. E.; St. John, J.; Boyd, S. E.; Brown, C. L.; Li, Q. Yellow-Emitting Carbon Nanodots and Their Flexible and Transparent Films for White LEDs. *ACS Appl. Mater. Interfaces* **2016**, *8*, 33102−33111.

(22) Agalave, S. G.; Maujan, S. R.; Pore, V. S. Click Chemistry: 1,2,3-Triazoles as Pharmacophores. *Chem. - Asian J.* **2011**, *6*, 2696−2718.

(23) Hilimire, T. A.; Chamberlain, J. M.; Anokhina, V.; Bennett, R. P.; O, S.; Myers, J. R.; Ashton, J. M.; Stewart, R. A.; Featherston, A. L.; Gates, K.; Helms, E. D.; Smith, H. C.; Dewhurst, S.; Miller, B. L. HIV-1 Frameshift RNA-Targeted Triazoles Inhibit Propagation of Replication-Competent and Multi-Drug-Resistant HIV in Human Cells. *ACS Chem. Biol.* **2017**, *12*, 1674−1682.

(24) Yan, J.; Fang, H.; Wang, B. Boronolectins And Fluorescent Boronolectins: An Examination Of The Detailed Chemistry Issues Important For The Design. *Med. Res. Rev.* **2005**, *25*, 490−520.

(25) O'Keefe, B. R.; Giomarelli, B.; Barnard, D. L.; Shenoy, S. R.; Chan, P. K. S.; McMahon, J. B.; Palmer, K. E.; Barnett, B. W.; Meyerholz, D. K.; Wohlford-Lenane, C. L.; McCray, P. B. Broad-Spectrum In Vitro Activity And In Vivo Efficacy Of The Antiviral Protein Griffithsin Against Emerging Viruses Of The Family Coronaviridae. *J. Virol.* **2010**, *84*, 2511−2521.

(26) Li, H.; He, X.; Kang, Z.; Huang, H.; Liu, Y.; Liu, J.; Lian, S.; Tsang, C. H. A.; Yang, X.; Lee, S.-T. Water-Soluble Fluorescent Carbon Quantum Dots and Photocatalyst Design. *Angew. Chem., Int. Ed.* **2010**, *49*, 4430−4434.

(27) Shen, P.; Xia, Y. Synthesis-Modification Integration: One-Step Fabrication of Boronic Acid Functionalized Carbon Dots for Fluorescent Blood Sugar Sensing. *Anal. Chem.* **2014**, *86*, 5323−5329.

(28) Wang, Y.; Lu, L.; Peng, H.; Xu, J.; Wang, F.; Qi, R.; Xu, Z.; Zhang, W. Multi-Doped Carbon Dots With Ratiometric Ph Sensing Properties For Monitoring Enzyme Catalytic Reactions. *Chem. Commun.* **2016**, *52*, 9247−9250.

(29) De Moor, J. E.; Van Der Kelen, P. Studies On Trivalent Boron Compounds II. Dipole Moment Measurements. *J. Organomet. Chem.* **1967**, *9*, 23−29.

(30) Beachell, H. C.; Beistel, D. W. Nuclear Magnetic Resonance Spectra of Phenylboronic Acids. *Inorg. Chem.* **1964**, *3*, 1028−1032.

(31) Good, C. D.; Ritter, D. M. Alkenylboranes. II. Improved Preparative Methods and New Observations on Methylvinylboranes. *J. Am. Chem. Soc.* **1962**, *84*, 1162−1166.

(32) Wang, Y.; Lu, L.; Peng, H.; Xu, J.; Wang, F.; Qi, R.; Xu, Z.; Zhang, W. Multi-Doped Carbon Dots With Ratiometric Ph Sensing Properties For Monitoring Enzyme Catalytic Reactions. *Chem. Commun.* **2016**, *52*, 9247−9250.

(33) Zhu, S.; Meng, Q.; Wang, L.; Zhang, J.; Song, Y.; Jin, H.; Zhang, K.; Sun, H.; Wang, H.; Yang, B. Highly Photoluminescent Carbon Dots For Multicolor Patterning, Sensors, And Bioimaging. *Angew. Chem., Int. Ed.* **2013**, *52*, 3953−3957.

(34) Khanal, M.; Vausselin, T.; Barras, A.; Bande, O.; Turcheniuk, K.; Benazza, M.; Zaitsev, V.; Teodorescu, C. M.; Boukherroub, R.; Siriwardena, A.; Dubuisson, J.; Szunerits, S. Phenylboronic-Acid-Modified Nanoparticles: Potential Antiviral Therapeutics. *ACS Appl. Mater. Interfaces* **2013**, *5*, 12488−12498.